PHILOSOPHICAL TRANSACTIONS A

royalsocietypublishing.org/journal/rsta

Research

Cite this article: Filipot J-F *et al*. 2019 La Jument lighthouse: a real-scale laboratory for the study of giant waves and their loading on marine structures. *Phil. Trans. R. Soc. A* **377**: 20190008.
http://dx.doi.org/10.1098/rsta.2019.0008

Accepted: 8 June 2019

One contribution of 14 to a theme issue 'Environmental loading of heritage structures'.

Subject Areas:
oceanography, ocean engineering, structural engineering, fluid mechanics

Keywords:
extreme wave, wave breaking, wave loading

Author for correspondence:
J.-F. Filipot
e-mail: jean.francois.filipot@ite-fem.org

Electronic supplementary material is available online at https://doi.org/10.6084/m9.figshare.c.4567532.

THE ROYAL SOCIETY PUBLISHING

La Jument lighthouse: a real-scale laboratory for the study of giant waves and their loading on marine structures

J.-F. Filipot[1], P. Guimaraes[2], F. Leckler[2], J. Hortsmann[3], R. Carrasco[3], E. Leroy[4], N. Fady[4], M. Accensi[5], M. Prevosto[5], R. Duarte[1], V. Roeber[6], A. Benetazzo[7], C. Raoult[2], M. Franzetti[8], A. Varing[1] and N. Le Dantec[4]

[1]France Energies Marines, Plouzané, Bretagne, France
[2]Service Hydrographique et Oceanographique de la Marine, Brest, Bretagne, France
[3]Helmholtz-Zentrum Geesthacht HZG Campus Teltow, Geestacht, Germany
[4]CEREMA Direction territoriale Ouest, Plouzané, Bretagne, France
[5]Ifremer, Plouzané, Bretagne, France
[6]University of Pau and Pays de l'Adour, Bidart, France
[7]CNR-ISMAR, Venice, Italy
[8]IUEM-LGO, Plouzané, Bretagne, France

J-FF, 0000-0003-0875-8791

This paper presents results from an experiment designed to improve the understanding of the relationship between extreme breaking waves and their mechanical loading on heritage offshore lighthouses. The experiment, conducted at La Jument, an iconic French offshore lighthouse, featured several records of wave, current and structure accelerations acquired during severe storm conditions, with individual waves as high as 24 m. Data analysis focuses on a storm event marked by a strong peak in the horizontal accelerations measured inside La Jument. Thanks to stereo-video wave measurements synchronized to the acceleration record we were able to identify and describe the breaking wave responsible for this intense loading. Our observations suggest that this giant wave (19 m high) had a crest elevation high enough to directly hit the lighthouse

tower, above the substructure. This paper reveals the potential for conducting ambitious field experiments from offshore lighthouses in order to collect valuable storm waves and wave loading observations. This offers a possible second service life for these heritage structures as *in situ* laboratories dedicated to the study of the coastal hydrodynamics and its interaction with marine structures.

This article is part of the theme issue 'Environmental loading of heritage structures'.

1. Introduction

(a) La Jument lighthouse: context

Offshore lighthouses at sea represent examples of engineering marvels, by overcoming challenges of constructing robust structures to withstand the extreme environmental loading they have to face for decades or even centuries. Among these environmental forcings, the wave loading generally dominates by far the winds or current actions on the structure. Indeed, because the lighthouses at sea are constructed upon shallow rocky platforms they are exposed to breaking waves responsible for intense and transient forces, also known as 'slamming' impacts. During the most extreme storms, breaking waves impacts threaten the lighthouses' structural integrity, which raises the question of the remaining lifetime of these fascinating monuments. Among the threatened offshore lighthouses, La Jument, located offshore of Ushant island, Western Brittany, France (figure 1) is one of the most iconic. A series of pictures taken from a helicopter by Jean Guichard, showing the lighthouse keeper opening the door while a giant wave engulfs the substructure is famous worldwide. La Jument's photogenic quality is tightly related to its extreme exposure to North East Atlantic storm waves. These waves that shoal over the very steep foreshore bathymetry may violently break over the lighthouse and generate sea spray that can run up well over the lighthouse lantern (see the helicopter video recording available as electronic supplementary material).

La Jument was completed in 1911 after 8 years of construction. The final structure, 48 m high above chart datum (CD), underwent worrying vibrations during the first strong winter storms. In 1911 and 1916, two storms were responsible for vibrations so intense that they caused the lantern glass to break and the mercury tank (supporting the Fresnel lens rotation) to overflow, forcing the lighthouse keepers to retrieve the toxic liquid with their bare hands [1]. These incidents pushed the engineers to propose and provide reinforcement of the lighthouse substructure (figure 1). This did not completely stop the waves from damaging the lighthouse. In 1934, three holes were drilled from the substructure to 30 m down to anchor La Jument directly into the underlying rocky platform.

Today, La Jument still faces storm waves and the question of the remaining lifetime of this iconic heritage monument is open. The same question, applicable to English rock lighthouses sparked interest in the scientific community. Considerable efforts were conducted through the STORMLAMP project (e.g. [2,3]) to improve the knowledge of the current mechanical response and health status of different British lighthouses exposed to high seas. Regarding La Jument [4] has addressed the complex question of the remaining lifetime of the structure and the possible reinforcements required to extend it. This in-depth study examined the mechanical structure's response to impacts of large breakers and showed that the lighthouse behaviour in terms of accelerations, displacements, strains and failures was highly correlated to the characteristics of the breaking waves hitting the lighthouse. However, knowledge of the wave field around La Jument was insufficient at the time of Loraux's work and he had to rely on wave climatology produced by a phase averaged spectral wave model to define the geometric and kinematic characteristics of the breaking waves for his extreme loading cases on La Jument. He concluded that dedicated field measurements would be valuable to support his results; this statement was part of the motivation for the experiment that will be described in this paper.

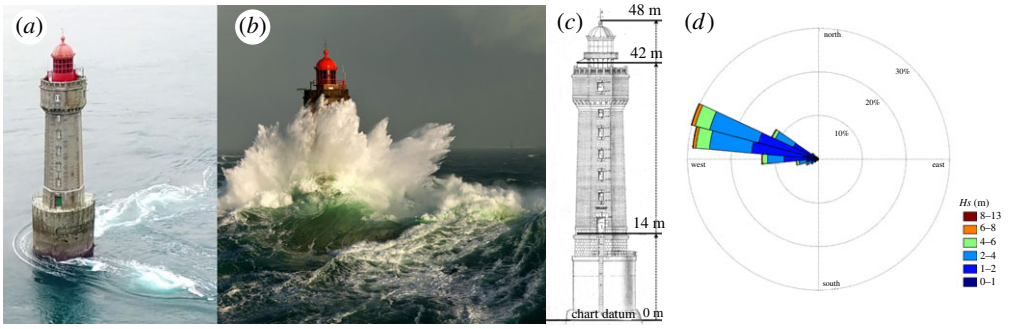

Figure 1. La Jument lighthouse, Brittany France (48°25′20.00″ N, 5°8′2.28″ W). (*a*) in calm wave conditions but with intense spring tide currents causing eddies in the wake of the lighthouse. The substructure added to the lighthouse to solve its early-life stability issues is well visible. (*b*) La Jument in storm conditions. Picture courtesy of Jean Guichard. (*c*) Historical plan of La Jument, before the addition of the final substructure. The current elevation above chart datum of the substructure is virtually shown here (14 m) as it is a key element for the paper. (*d*) Wave rose from the wave climatology presented in the paper (location of the extraction: 48°25′35″ N, 5°7′50″ W, i.e. about 1.2 km in the northwest of La Jument).

(b) Lighthouses design and breaking waves

The design of any marine structure, such as offshore oil platforms, offshore wind turbines, breakwaters or offshore lighthouses, relies among other parameters on knowledge of the most extreme sea states that the structure will possibly face over its lifetime. The corresponding characteristic 100 or 50 year wave is then used to compute inertia and drag forces based on Morison theory [5]. It is now well acknowledged that in the presence of breaking waves, an additional impact or slamming force should be added. Indeed, at breaking onset, the horizontal fluid velocities at the wave crest reach or even exceed the wave phase speed. At breaking onset, the wave crest (or at least part of it) behaves as a wall of water moving at the wave crest phase speed and its encounter with a marine structure results in a violent impact, yielding a large impulsive force. This breaking wave impact force must be considered in the marine structure design since it can be several times greater than the magnitude of the combined drag and inertia forces, though over a very short time interval [6]. The severity of the breakers and hence the magnitude of their induced force on the structures depends on the type of breaking (e.g. [7]): the most gentle ones, known as spilling breakers are initiated by a modest jet located in the direct vicinity of the wave crests, while plunging breakers are characterized by a much larger and more intense jet, enclosing an air pocket during the process of breaking. In addition, irrespective of the breaking type, the stage of the breaking process at impact is an important parameter, namely a broken wave with its highly aerated front face will cause a lower impact force than a wave at breaking onset, featuring a non-turbulent, non-aerated, vertical front face with high fluid velocities in the wave propagation direction (e.g. [8–10]).

When and why waves are breaking remains an open question because the understanding of wave breaking physics is still poor. For instance, until recently there was no consensus regarding an universal breaking onset criterion for irregular waves. Among the pioneers in this field, Miche [11] demonstrated that regular waves over a flat bottom are stable until $kH/\tanh(kd) = 0.88$, where k is the wavenumber, H is the wave height and d is the water depth. In deep water, this leads to the familiar $H/L = 1/7$ threshold in which $L = 2\pi/k$ the wavelength of an individual wave. In shallow water the Miche breaking limit becomes the so-called 'breaker index' $H/d = 0.88$, while the most widely used value is 0.78 [12]. Miche theory is not directly applicable to irregular waves propagating over a possibly varying bottom. A paper from Barthelemy *et al*. [13] suggests that any deep or intermediate water wave with a ratio orbital velocity at the crest over phase speed greater than 0.85 will inevitably and quickly break (within a fraction of wave period). Preliminary results

from Varing *et al*. [14] indicate that this breaking limit could be valid in shallow water as well. Shallow water breaking waves have been widely discussed in the literature and as mentioned above, it is well known that breaking onset can be related to the breaker index H/d. Thornton & Guza [15] showed that at a given location (or water depth) the probability density function of breaking wave height was not a Dirac function but a rather broad distribution. This is due to the stochastic nature of the breaking occurrence and probably to measurement technique that detects breakers at different stages. In addition to the height of the breakers, the type of breaking controls the magnitude of the wave loads on marine structures. The well-known Iribarren or surf similarity parameter [16], $\zeta = \tan\beta/\sqrt{S_0}$, with β being the bottom slope and S_0 being the deep water wave steepness, provides an empirical breaking type classification. For storm waves at La Jument, ζ takes values between 2 and 3, typical of plunging waves. This is further consistent with visual observations of storm waves in the vicinity of La Jument. As explained in this paragraph, the knowledge regarding breaking waves statistics and type is still empirical and its application to complex and extreme hydrodynamic conditions found at La Jument is somewhat cumbersome. This stresses the importance of collecting direct and detailed observations of breaking waves on this site.

Because of the associated short impulsive force, breaking waves can excite specific structural modes of marines structures including lighthouses or offshore wind turbines. For instance, Hallowell *et al*. [17] noted that only breaking waves were able to excite the second mode of oscillations of a 2 MW fixed offshore wind turbine deployed at the Blyth wind farm (UK). Chella *et al*. [18] reported that the large remaining uncertainties in the design of offshore wind turbines are connected to our lack of knowledge of the breaking waves loading. The pioneering work from Von Karman [19] assimilated the effect of a breaking wave to the impact of a cylinder falling and hitting the water surface. Later, Goda & Kakizaki [20] concluded that the breaking-induced wave force on a vertical cylinder is due the change in momentum in the water mass. More recently, Wienke & Oumeraci [21] proposed the following expression for the time evolution of the slamming force induced by a breaker over a vertical cylinder:

$$F(t) = \lambda \eta_c \rho_w R V^2 \left(2\pi - 2\sqrt{\frac{V}{R}t}\tanh^{-1}\sqrt{1-\frac{V}{4R}t} \right), \tag{1.1}$$

for $0 \le t \le R/8V$,

$$F(t') = \lambda \eta_c \rho_w R V^2 \left(\pi\sqrt{\frac{V}{6Rt'}} - \left(\frac{8V}{3R}t'\right)^{1/4}\tanh^{-1}\sqrt{1-\frac{V}{R}t'\sqrt{\frac{6V}{R}t'}} \right), \tag{1.2}$$

for $(R/8V) \le t' \le (12R/32V)$, with $t' = t - R/32V$.

The parameters controlling the intensity and time distribution of the impact force are therefore η_c the elevation of the crest above the mean sea level, λ the curling factor that gives the portion of the crest impacting the structure, V the orbital fluid velocity in the crest, ρ_w the water density and R the radius of the cylinder. This formulation was carefully validated with a number of wave flume experiments reproducing the impact of breaking waves on a cylinder and is used in design standards for offshore marine structures (see, for instance, [22] for application to offshore wind turbines). Though the relevance of considering breaking waves for design purpose, the impact forces might also be considered for fatigue computations especially in shallow water environment (such as La Jument) where breaking waves are frequent [23]. From equations (1.1) and (1.2), it appears that the geometric and kinematic properties of the breaking waves (i.e. the parameters η_b, λ and V) determine the magnitude and time evolution of the slamming force. Unfortunately, it is very difficult, if not impossible, to infer the characteristics of the breaking waves at the moment of their impact from a typical wave climatology that usually provides integrated wave parameters computed at several hundreds metres away from the structure.

Table 1. Extreme Wave/Wind/Current statistics from HOMERE database, H_s is the significant wave height, U_{10} and $U_{10,d}$ are the 10 m-high wind speed and direction, respectively; T_p and D_p are the peak period and direction of waves, respectively; C_s and C_d are the current speed and direction, respectively.

	return values				most severe event						
	10y	20y	50y	100y	H_s (m)	T_p (s)	D_p (°)	U_{10} (m s^{-1})	$U_{10,d}$ (°)	C_s (m s^{-1})	C_d (°)
H_s (m)	11.8	12.7	13.9	14.7	12.7	17	−66	21.3	−78	0.79	146
U_{10} (m s^{-1})	27.2	28.3	29.4	30.0	9.9	13.5	−82	29.4	−70	0.33	131
C_s (m s^{-1})										0.92	323

(c) Objectives of the paper

In this paper, we shall try to provide a description of the hydrodynamic conditions at La Jument with a focus on the breaking waves impacting the lighthouse during storm events. The first part of the paper describes the storm waves, current and structure acceleration observations and bathymetric data collected from or around this lighthouse during winter 2017–2018. The second part of the paper focuses on a particular storm event on 3 January 2018 marked by a strong and transient acceleration and displacement peak in the lighthouse at 9:42:07 UTC, induced by a giant breaker slamming over La Jument. A discussion follows on the characteristics of this wave to elucidate why it produced considerably higher accelerations and displacements of the structure compared to the other large waves of the same storm event.

2. Hydrodynamic climate around La Jument

The lighthouse is located in a macro-tidal environment. Tidal observations were recorded in 2013 by SHOM in the Lampaul bay (5°06′ W, 48°27′ W) and were analysed in [24]. The tidal range is 7.68 m and mean level is 4.13 m CD. Harmonic analysis on water elevation was also computed and tidal predictions from them are used in the paper. The tidal currents around La Jument can exceed 2 m s^{-1} and have a complex horizontal distribution (figure 3). An analysis of the extreme statistics at La Jument was produced based on the 23 years (1994–2016) of the hindcast database HOMERE [25]. The selected model point (48°25′35″ N, 5°7′50″ W) for the extreme statistical analysis is located northwest of La Jument, about 1260 m away from the lighthouse. At that location the water depth is 39 m with a tidal range of 6.8 m. A blockmax method with a block duration of one month was used to estimate the distribution of the yearly maximum water level. The fit on the monthly maxima by a Gumbel distribution gives 11.8 m for a return period of 10 years. The significant wave height, H_s and current speed, C_s (only tidal current in HOMERE) are not correlated. The dominant directions of waves for $H_s > 9$ m are 250°–300° (approx. WSW to WNW; table 1).

3. Description of the field experiment

(a) La Jument experiment

(i) Context

This experiment was performed within the frame of the DiMe project dealing with the characterization of extreme breaking waves for the purpose of survivability design of marine renewable energy devices such as fixed or floating wind turbines or wave energy converters. Because the observation of extreme sea states is cumbersome due to the obvious hazards faced by any instruments deployed in stormy seas, little is known about their characteristics and especially

regarding their breaking properties (e.g. statistics of occurrence, breaking type). This motivated the acquisition of oceanic storm wave observations with a focus on the breaking waves.

La Jument lighthouse was chosen for the study of extreme breaking sea states for the following reasons:

(i) The lighthouse lies over a rocky platform that drops abruptly on its western boundary.
(ii) The upper deck of the lighthouse is located at about 42 m above the CD, making possible the observation of very high sea states in intermediate to shallow waters with a large field of view and a minimal shadowing effect.
(iii) Its high location provides a (relative) shelter from the extreme sea states for onsite remote sensing instruments.
(iv) An analysis of the HOMERE database [25] shows that the 10 year significant wave height at La Jument (in 50 m depth) is equal to or larger than the 100 year significant wave height of most of the French Channel and Atlantic coastline.
(v) In the meantime, a parallel experiment had been planned to measure the acceleration of the lighthouse under storm wave impacts, based on the recommendations of [4].

The connection between the storm waves field experiment and the acceleration measurements appeared to be relevant and motivated the writing of the present paper.

(ii) Instruments deployment

The deployment of an X-band radar, Stereo-Video Imagery system (SIS) and four accelerometers on La Jument took place on 5 and 6 December 2017. Because the access to the lighthouse by sea is hazardous, especially in winter, we relied on the civilian security helicopter to reach La Jument. Previously, a wave buoy and a current profiler were moored during the winter by the French Naval Hydrographic and Oceanographic Service (Shom) to independently measure the offshore wave field and current vertical profile. Finally, a bathymetric survey was performed in July 2018 to improve the knowledge of the water depth around the lighthouse. In the next section, we will be described the instrumental set-up involved in this field experiment.

(iii) Stereo video system

The stereo-video cameras were mounted on each side of a hut located just below the lantern and looking approximately 246° N. SIS used in this experiment consists of a pair of synchronized 5 megapixel (2048 × 2456 pixels) BM-500GE JAI cameras, with a 5 mm and wide angle lens. The cameras synchronization was done by a trigger inside of the left camera case, the maximum difference between the two cameras records were of the order of $O(10^{-5})$ s. The configuration of the lighthouse imposed a maximum camera separation (baseline) of 5.44 m. The stereo images acquisition rate was set at 10 Hz and time stamped thanks to a GPS time server. The cameras were deployed at about 42 m above the CD and equipped with sprinklers and wipers enabling them to be cleaned before each acquisition and during extreme sea states conditions. This system collected 7 TB of storm waves, corresponding to about 35 h of observations between 6 December 2017 and January 15 with significant wave height reaching 10.5 m. The sea surface reconstruction method used follows the methodology presented by Fedele [26], Benetazzo [27] and Leckler [28] implemented in the WASS (waves acquisition stereo system) code version 1.4, from [29].

The sea surface area covered by the stereo video images and the surface resolution mostly depend on the experimental set-up, local brightness and sea level position. The expected accuracy of the stereo observations was derived using the formulations of the quantization error from [30]. For the present stereo set-up, the expected quantization error is represented by the root-mean-squared (RMS) errors along the x-, y- and z-axes. This set-up allowed one to capture the wave field at 50 m from the base of the tower up to 250 m offshore, with a RMS$x = 0.14$ m, RMS$y = 0.35$ m and RMS$z = 0.09$ m.

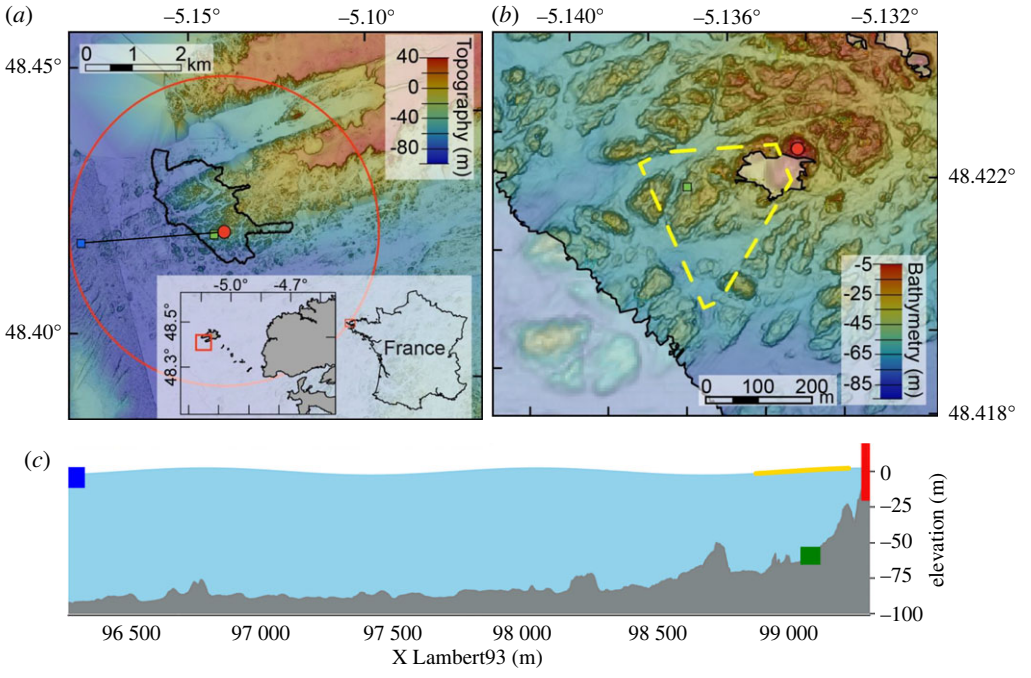

Figure 2. Bathymetry around La Jument. (*a*) Global view, La Jument position is marked by the red dot. The blue and green squares display the location of the Datawell wave buoy and AWAC current profiler. The red circle indicates the domain covered by the X-band radar. The bold black line shows the area covered by the bathymetric survey conducted in the project and the black straight line corresponds to the profile presented in the lower panel. (*b*) Zoom on La Jument bathymetry. The green square is the AWAC position and the dashed yellow line encloses the stereo video reconstruction domain. The blurred area corresponds to pre-existing bathymetric data. (*c*) A schematic bathymetric profile between lighthouse (red vertical bar on the right) and Datawell buoy (blue square on the left). The yellow line on the surface represents the stereo video field of view and the green square is the AWAC position. The profile is in Lambert93 coordinate system, in a metric scale.

The main source of error observed in the system was related to the correlation around the breaking events. Breaking waves form bright patches over darker surface water, sometimes resulting in strong brightness gradients that disturb the reconstruction process. The correlation around the foam patches was improved by Leckler [28]; however, this is still one of the main restrictions in the stereo-video reconstruction. Therefore, the analysis of the wave field in the direct vicinity of the lighthouse was performed with extra care because of the presence of larger breakers.

(iv) X-band marine radar

All radar data used within this study were acquired by a 12 kW marine radar, operating at X-band (9.3 GHz) with vertical polarization in transmit and receive modes (VV-pol). The radar was mounted at a height of about 43 m.a.s.l. and run in a rotational mode covering a range of roughly 3260 m at 0.5 Hz around the lighthouse (red circle in figure 2). The radar was operated with a pulse length of 50 ns, which resulted in a range resolution of 7.5 m. The antenna had a vertical beam opening of 21° and a width of 7.5 feet (2.3 m) giving an azimuthal resolution of approximately 0.9°. The radar was run with a pulse repetition frequency of 2 kHz and the backscattered signal operated through a linear amplifier and then was digitized with 13 bits.

Within this experiment, the X-band marine radar was used to observe ocean waves in space and time. This allows the measurement of the two-dimensional wave spectra from which parameters such as the peak wave direction and peak wave period can be determined [31,32]. In

addition, the radar data give surface wave properties such as wavelength and phase velocity, which in turn enable one to retrieve the surface current vector [33,34]. The surface currents measurements result from the difference between the observed phase velocity and that given by the linear dispersion relation of surface gravity waves, which is given by

$$\omega(\mathbf{k}) = \sqrt{gk\tanh(kd)} + \mathbf{k}\cdot\mathbf{U} = \omega_0(\mathbf{k}) + \mathbf{k}\cdot\mathbf{U}, \tag{3.1}$$

where $\mathbf{k}$ is the wavenumber vector, ω and ω_0 the relative and absolute wave pulsation, g the gravitational force, d the water depth and $\mathbf{U}$ the two-dimensional near-surface current. A detailed description of the methodology used in this study to extract the surface current fields is described in [35]. An in-depth validation of surface currents retrieved by marine radars showed an RMSE of less than $0.04\,\mathrm{m\,s^{-1}}$ [36].

(v) Accelerometers

The four RECOVIB-IAC-A03 accelerometers were firmly mechanically fixed inside the lighthouse at four different heights: 20.6, 31.1, 38.7 and 45.6 m above the CD. The highest one is installed on the steel structure that supports the lens close to the top of the lighthouse while the three remaining are mounted on the inside masonry of the lighthouse. These accelerometers are able to measure accelerations in the range $\pm 2g$ (with g the gravity acceleration) outputting a current of 4–20 mA. They embed a low-pass filter of first order with an upper frequency limit of 1000 Hz (−3 dB). The accelerometers were wired to a data acquisition system which is independent of the one used for radar and cameras but synchronization with the wave observations was still possible thanks to GPS time stamping. The power consumption of these systems was very low compared with the other devices deployed for the experimentation so that it was possible to record all the data throughout the winter. The data acquired at 5 kHz were stored in the lighthouse in a dedicated hard drive and transferred on an hourly basis to the mainland to allow preliminary analyses without physical access to the lighthouse.

(vi) Bathymetric campaign

Bathymetric information was lacking in the immediate vicinity of La Jument, even though it was critical for understanding and modelling wave propagation and wave breaking around the lighthouse. Water depth close to the lighthouse is beyond bathymetric Lidar capabilities due to the steep seabed slope near the lighthouse, and the strong tidal currents and high waves make this zone of rocky shoals very difficult for marine navigation (numerous shipwrecks). To fill the lack of high-resolution bathymetric data in the vicinity of La Jument, we conducted a field campaign in July 2018, with the research vessel (R/V) 'Albert Lucas'. The hydrographic survey was carried out with a shallow-water multibeam echosounder (MBES) Kongsberg EM3002 (high-resolution 300 kHz MBES system) coupled with a hull sound velocity sensor (H-SVS) Valeport miniSVS, an inertial measurement unit IxSea Octans3000 and a global navigation satellite system (GNSS) Astech ProFlex500. Sound velocity profiles were carried out with an AML BaseX equipped with sound velocity and pressure sensors of model Xchange. The GNSS navigation was processed according to the post processed kinematic method with Novatel GrafNav software and the multibeam soundings were edited with QINSy software, in order to provide a 2 m grid digital terrain model.

(vii) Wave and current *in situ* measurements

To complete the field campaign, one directional Datawell waverider wave buoy and an acoustic wave and Nortek AWAC current profiler were deployed in the vicinity of the lighthouse on 27 November 2017. The wave buoy was located about 3 km away from the lighthouse (5°10.410′ W, 48°25.131′ N) in the western direction, at 92 m depth and at the limit of the radar coverage (figure 2). The wave buoy was deployed on 27 November 2017 and recorded until 3 March 2018. The current profiler was deployed at 59 m depth CD, about 300 m away from the

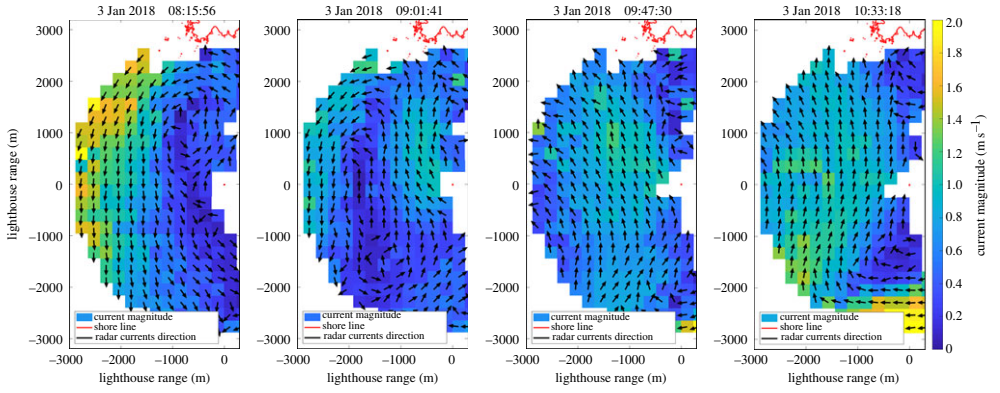

Figure 3. Marine radar retrieved current maps of 3 January 2019 between 08.15 and 10.30 UTC (left to right). The colour coding gives the current magnitude and the unit vectors represent the current directions. Each map was generated from 15 min of marine radar data.

lighthouse (5°08.196′ W, 48°25.284′ N) in the southwest direction, at the limit of the video-system reconstruction area (figure 2). The AWAC stopped its acquisition on 1 February 2018 and was found to be seriously damaged on the inter-tidal area on the north shore of Ushant island two months later. The analysis of the data revealed that the instrument was not stable on the bottom with tilt values of up to 40° due to ebb currents. Accordingly, we kept only the data acquired in the tilt validity range given by the instrument manufacturer. More than 60% of the AWAC records were removed, mainly during ebb tides.

4. Results

(a) Bathymetry

Figure 2 shows the bathymetry surrounding La Jument. The lighthouse stands on a promontory that is always submerged except during low spring tides. Our high-resolution bathymetry reveals with greater details the densely fractured bedrock on the barren platform that is extending 2–3 km away to the west and south of the lighthouse. Except for the area north of La Jument, as well as in the bedrock fractures, there is no sediment cover on the granitic bedrock, consistent with high-energy hydrodynamic conditions. Secondary fractures also occur oblique to the main fault orientation. The dense network of fractures yields a rather chaotic seabed relief with large blocks separated by deep incisions. The waves that we will describe in the rest of the paper are propagating approximately from west nothwest, hence will advance towards the lighthouse over this indented topography. The bathymetry data collected here are therefore of primary importance when examining the wave physical processes (refraction, shoaling and breaking) that will control wave loads on La Jument.

(b) X-band radar observations

The marine radar, which retrieved current fields from 3 January 2018 between 08.15 and 10.30 AM UTC, are shown in figure 3. Each current map results from approximately 15 min of radar data. The window size for the retrieval of each current vector is 480 × 480 m and adjacent cells are overlapping by 50%, which leads to one current vector every 240 m. For the current field retrieval only wavelengths between 15 and 100 m were considered, which give access to the mean current in the upper 7 m. Figure 3 shows the current field at different instants close to the time of the waves and accelerations records that are discussed in detail in the rest of the paper. It reveals a complex horizontal distribution of the current field with velocity magnitude reaching 1.8 m s^{-1} over the

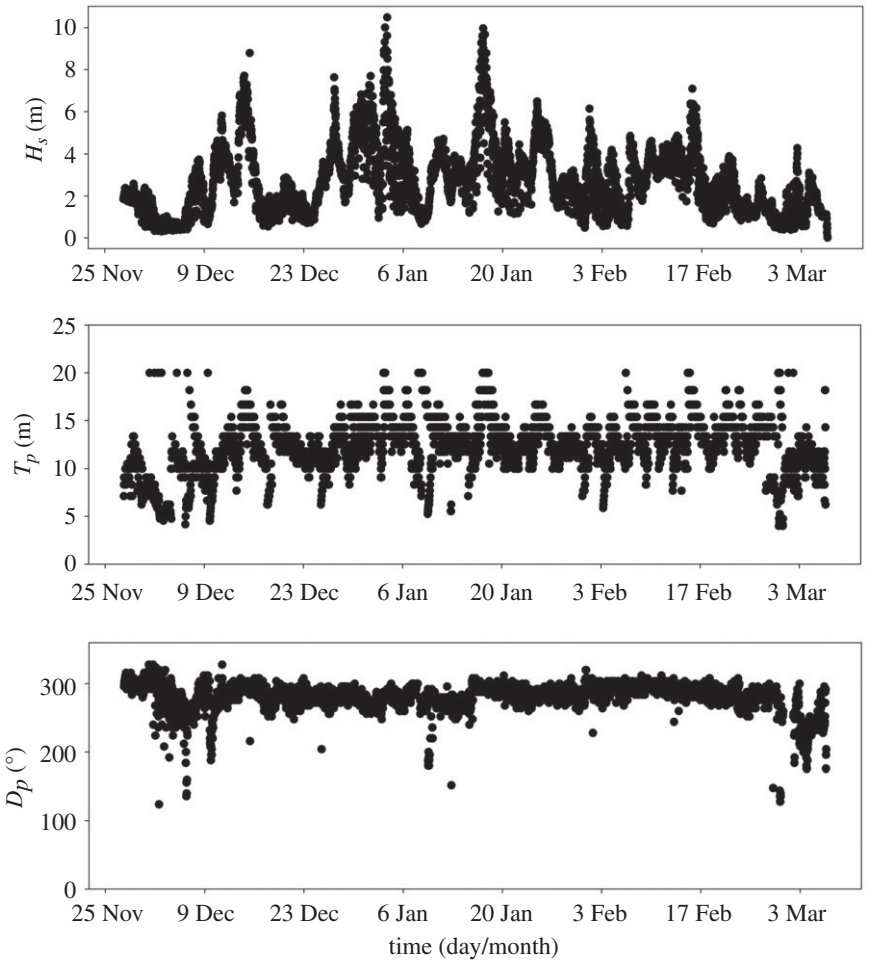

Figure 4. Time series of the significant wave height H_s, peak period, T_p and peak wave direction, D_p measured by the offshore wave buoy moored during winter 2017–2018.

domain of interest and about $1\,\mathrm{m\,s^{-1}}$ in the area covered by the SIS of La Jument at the time (09:47:30 UTC, third panel of figure 3) close to the wave event considered in the rest of the paper.

(c) Wavebuoy observations

The wavebuoy provided wave spectra every 30 min from which integrated wave parameters were extracted. Strong currents caused the buoy to malfunction episodically, the corresponding data were filtered out for the analysis. Figure 4 displays the time history of the significant wave height H_s which shows intense storm waves with H_s values close to 10 m as for instance the storm event of 3 and 4 January 2018 that is studied in the present paper. During storm events, typical peak period and wave direction values are about 15 s and 270° N, respectively.

(d) Stereo video observations

Owing to technical issues, the SIS stopped working from 15 January 2018. During it operation phase, the SIS captured several wave records in storm conditions with significant wave height ranging from 7.5 to 10.5 m (table 2).

Table 2. Summary of the storm records captured by the SIS during the field experiment. The date marks the time when the SIS acquisition starts (duration: 30 min each). The significant wave height (H_s) and peak wave period (T_p) for each event is measured by the stereo video system, the peak wave direction (D_p) is that of the Datawell (i.e. without the bathymetry effect), the mean current speed C_s is measured from the X-band radar and the wind speed at 10 m height (U_{10}) is estimated using the wind hindcasts from European Centre for Medium-Range Weather Forecasts (ECMWF) for La Jument location.

date	H_s (m)	T_p (s)	D_p (°)	C_s (m s^{-1})	U_{10} (m s^{-1})
3 Jan 2018 09.39	10.03	13.3	279	0.77	17.9, W
3 Jan 2018 10.30	10.51	15.4	278	0.69	15.5, W
3 Jan 2018 11.09	8.33	12.5	282	0.36	15.5, W
3 Jan 2018 11.54	9.63	12.5	281	1.08	15.5, W
4 Jan 2018 09.40	7.34	11.1	279	0.65	15.0, W
4 Jan 2018 10.45	7.18	10.5	286	0.79	14.7, W
4 Jan 2018 11.43	7.52	11.1	274	0.52	14.7, W

An analysis of the SIS surfaces for the record of 09.39 on 3 January 2018 (which will be analysed in more details later) revealed some interesting features about rogue wave occurrence in the vicinity of the lighthouse. For this analysis, only wave components of frequency higher than 0.5 Hz were selected, thus removing sparse spikes close to the poorly matched areas. Following the standard procedure, the dataset was analysed by splitting the sea surface region and the time interval in adjacent and non-overlapping subrecords [37]. To this end, we have selected 14 space–time regions V_s (with $s = 1, 2, \ldots, 14$) of same area $A_s = 12\,920\,\mathrm{m}^2$ and duration $D_s = 50\,\mathrm{s}$ in order to produce independent realizations of the random variable maximum crest height defined as $C_m = \max(z(x, y, t) \mid (x, y, t) \in Vs)$. As a result, the observed values of C_m range between 1.04 H_s and 1.76 H_s (on average $C_m = 1.31\ H_s$), and seven individual waves can be classified as rogue as they meet the classic criterion $C_m > 1.25\ H_s$ [38]. Two single waves exceeded 1.7 H_s (for comparison, the Draupner wave reached 1.55 H_s), the highest one, observed at about 80 m in the southwest of the lighthouse, peaked at 17.7 m.a.s.l. and had crest-to-trough height of about 24 m. Compared to typical open ocean waves, all crests are very steep (the crest-to trough half-period is about 0.4 T_p) and are accompanied by rounded and shallow troughs; the ratio between the lowest trough and the highest crest is 0.3, on average. These analysis performed on the SIS surfaces indicate that the occurrence rates of rogue waves at La Jument were higher than expected for deep water waves, possibly due to wave interaction with the bottom and or with the current field.

(e) Accelerometer observations

The goal of our experiment was to investigate the relationship between the incoming wave field and the mechanical loading felt by the tower in a wave-by-wave framework. To achieve this, we focused our efforts towards a deterministic comparison between the waves captured by our SIS and of the accelerations measured inside the lighthouse. One particularity of this experiment is the synchronization of the acceleration and SIS acquisition system (through the use of a time server, Galleon NTS-6002-GPS time server, accuracy 1 µs) that enabled us to connect a peak in acceleration to a wave captured by the SIS. Because of the slender geometry of the lighthouse, the accelerations induced by waves are larger at the top than near the base of the lighthouse hence the signal-to-noise ratio of the highest accelerometer is more favourable to examine the effect of waves on La Jument's mechanical response. For this accelerometer, the x-axis is pointed 214° N and the y-axis 124° N.

Figure 5 presents a sample of synchronized elevation and accelerations time series that were collected on 3 January between 09:39:38 and 10:09:38 UTC, containing the largest acceleration peak captured during the 3 and 4 January 2018 event. For our analysis, we extracted the

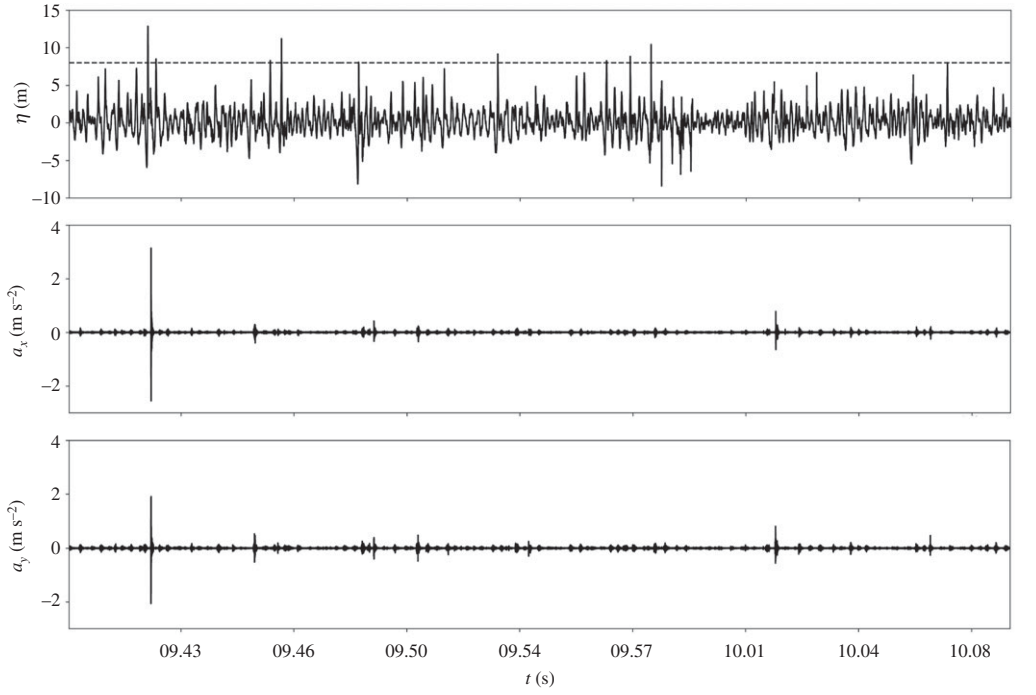

Figure 5. First panel, 30 min elevation time series for 3 January 2019 (starting at 09:39:38 UTC) extracted from point ($X = 99\,250$ m, $Y = 6844\,500$ m) in the stereo images of figures 7 and 8, the horizontal dashed line show the 8 m elevation threshold used to select the individual waves studied in the paper. Second and third panel: accelerations along *x*- and *y*-axes for the same record measured by the highest accelerometer in the tower. The signal noise was filtered out using a Butterworth filter with a cut-off frequency of 50 Hz.

wave elevation data from P_{SIS} the nearest point from the lighthouse, located at $X = 99\,250$ m, $Y = 6\,844\,500$ m (figures 7 and 8) hence about 50 m away, southwest of La Jument. Unfortunately, the white waters generated by breaking waves at the base of the lighthouse prevent any reliable stereo reconstruction closer to the structure due to a lack of texture in the images.

The horizontal displacements of the tower can further be computed from the acceleration records by double integration in time and is a better proxy to measure the possible structural damages since it is related to the strains in the structure as reported in Loraux's [4] study on La Jument. For the largest acceleration peak (about 3 m s^{-2} in the *x*-direction and 2 m s^{-2} in the *y*-direction) measured around 9:42:07 on 3 January the horizontal displacement reached a peak value of about 45 mm, a value several time higher than the other acceleration events presented in figure 5. This acceleration and displacement peak is related to an extreme wave (hereinafter referred to as 'wave1'), 19 m high with a crest elevation reaching 12.9 m at location P_{SIS}. In the next section, we will explore why this particular wave induced such an intense impact on La Jument.

(f) Focus on one extreme slamming wave

Video images of wave1, show a water vertical excursion consecutive to the wave slamming on the lighthouse that washed up the video cameras located about 41 m.a.s.l. (at that instant). This is illustrated by figure 6 showing the evolution of wave1 before and during the breaking process. Unfortunately, the stereo-video images do not give access to the impact zone of the wave on the structure as the video images do not cover the base of the lighthouse and because the white waters in the immediate vicinity of the lighthouse make stereo reconstruction inaccurate. A careful visual

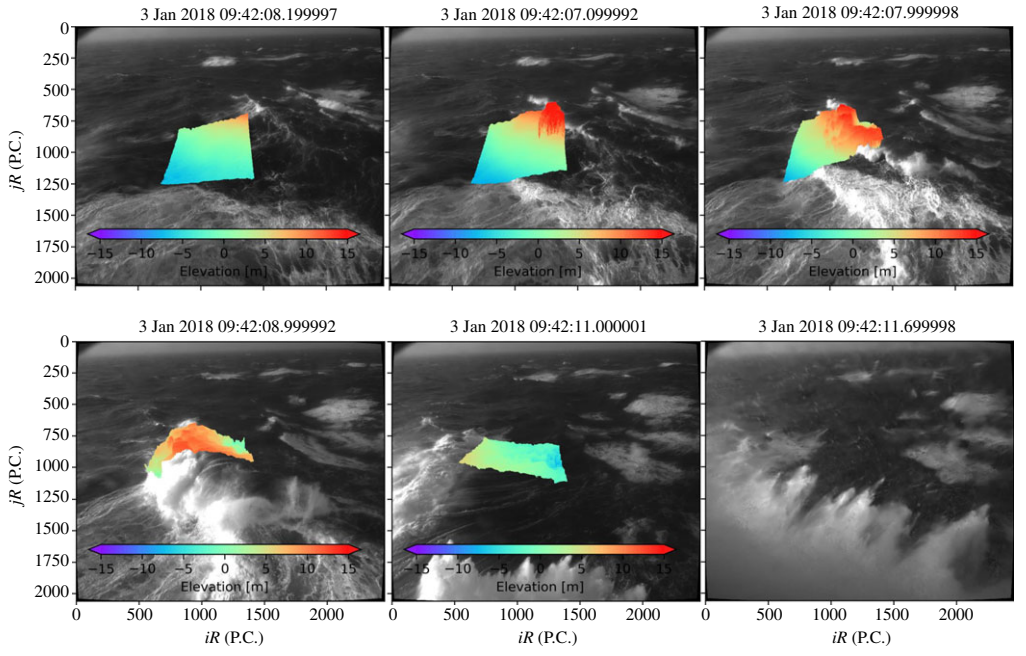

Figure 6. Examples of stereo video three-dimensional surface elevation map $z(iR, jR, t)$ plot over its corresponding right camera bitmap image in the pixel reference system. The colourbar shows the sea surface elevation and ranges from −15 m (blue) to +15 m (red) above the mean sea level computed at the time of the record. The sequence of images shows an extreme breaking event (referred to as wave1 in the paper, corresponding wave height: 19.0 m). The reconstruction area was reduced in this illustration to highlights the breaking areas.

analysis of the other video records (table 2) revealed that no other wave caused such water runup. In the following section, we compare wave1 to seven over waves from the same SIS record, whose crest elevations exceed a threshold set at 8 m.a.s.l. We chose to select our subset of high waves based on their crest elevation, η_c, instead of their trough-to-crest height because η_c appears to be a key parameter in the formula of [21] used to compute wave impact forces on slender bottom-mounted vertical-cantilever type marine structures (see equations (1.1) and (1.2)).

(i) Spatial wave properties analysis

Here we shall use a combination of the video images and of the stereo-video reconstruction to obtain a better description of the high waves of interest at the base of the lighthouse. The strength of the stereo-video system compared to other traditional point *in situ* wave instruments is of course its ability in providing spatio-temporal information on the wave field. Figures 7 and 8 display snapshots of the sea surface capturing the spatial signature of the eight high waves selected above. The photographs of these waves (figures 7 and 8, left panels) indicate that they were all breaking at the base of the lighthouse. Compared to the others, wave1 appears to have strong variation of the along-crest elevation, with high elevations concentrated close to the lighthouse. Snapshots of wave1's nonlinear evolution towards breaking is available in figure 6, and animations of the wave surfaces overlaid over the video images can be analysed to further understand the breaking process at the base of the lighthouse (these videos are available as electronic supplementary material; the reconstruction area was reduced in these videos to highlight the breaking areas). It reveals that when the wave crest is approaching the structure, a fast flow towards the crest appears and seems to be associated with the birth a secondary jet just below the main crest. Finally, both crests merge into one that violently overturns. Figure 8.6.a also shows a good illustration of the secondary jet generation.

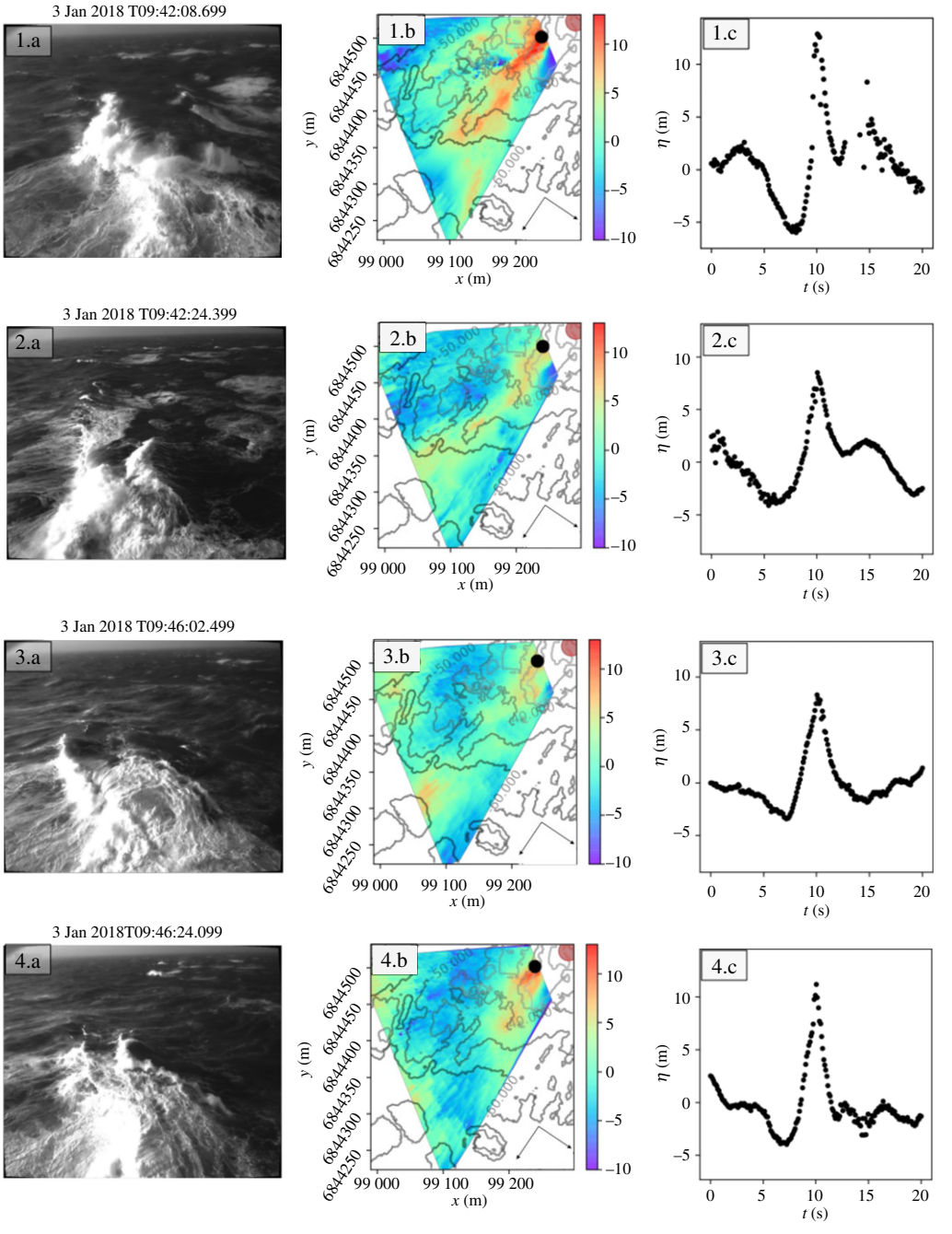

Figure 7. Description of the eight high waves selected for our study (four in this figure and four in figure 8). Left panels: video images, middle panel reconstructed wave surfaces projected in a Lambert93 geographic system overlaid over iso-contours of water depths (the black dots show the extraction point of the time series analysed in the paper) right panels: time series of the high waves elevation, collected at $x = 99\,250$ m, $y = 6844\,500$ m from the stereo video reconstruction.

(ii) Time-series analysis

We analysed the same surface by extracting a 30 min time series of the sea surface elevation recorded at P_{SIS}, for the same SIS acquisition (starting at 09:39:38 UTC). With this elevation time series, we pursue our investigations of the eight high waves properties. Superposing the

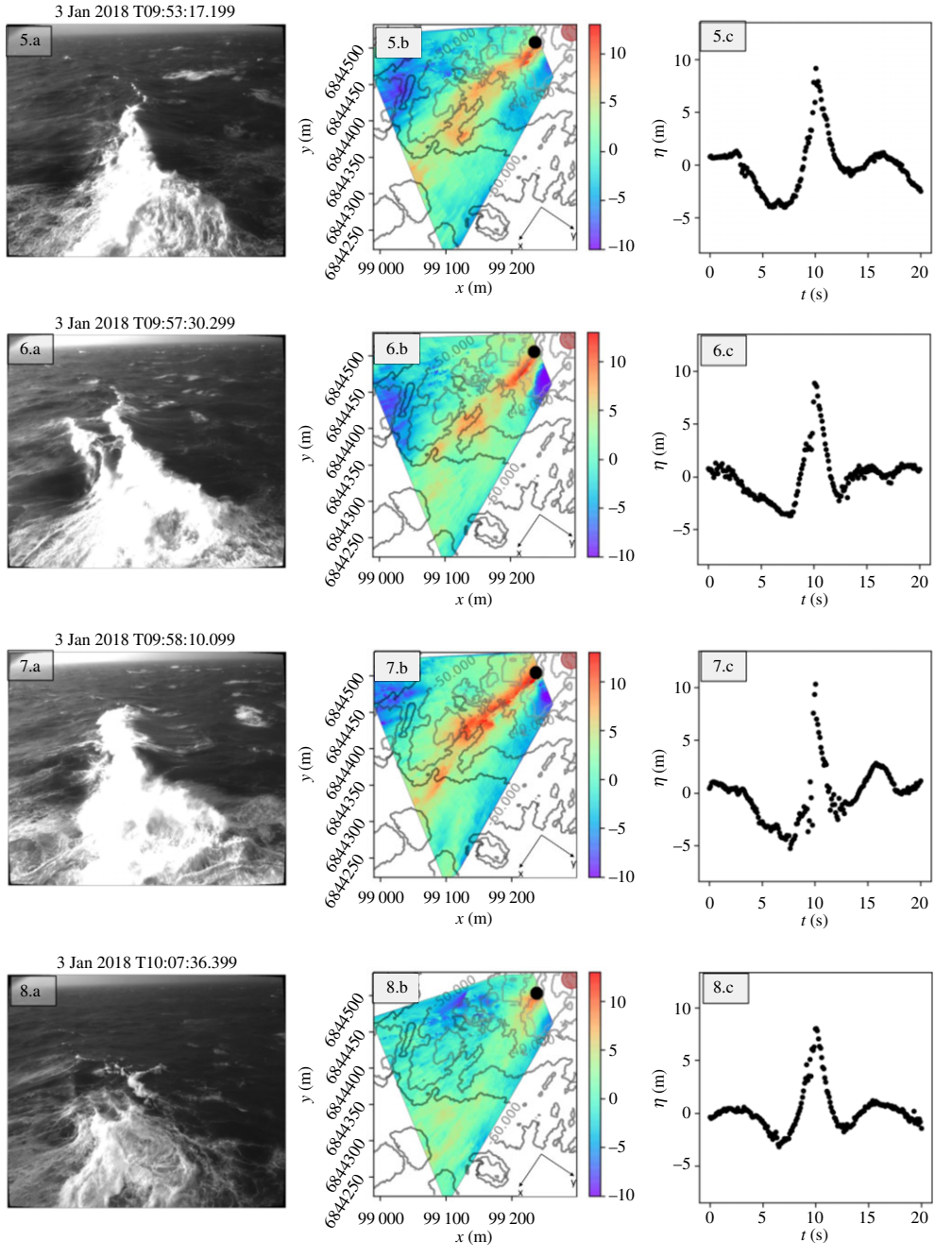

Figure 8. Same as figure 7 but for the four remaining high waves.

individual waves on a single plot shows time profile similarities between the eight high waves selected in terms of vertical and horizontal asymmetries. Some of the characteristics of these waves are listed in table 3.

Such similarities in the wave profile of high waves were already discussed for deep water waves by Bocotti [39], Phillips *et al*. [40,41], who proved that for Gaussian sea states, the profiles of the highest waves were self similar and follow the shape of the auto-correlation function of the full wave field. The eight high waves studied here are all skewed: the crests being much higher

Table 3. Crest, η_c and trough η_t elevation, wave height H and half period $T_{1/2}$ (duration between front trough and crest) for the eight individual waves studied in the paper.

wave	η_c (m)	η_t (s)	H (m)	$T_{1/2}$ (s)
wave1	12.9	−6.1	19.0	2.0
wave2	8.5	−4.1	12.6	4.6
wave3	8.3	−3.4	11.7	2.9
wave4	11.2	−4.0	15.2	2.8
wave5	9.2	−4.0	13.2	2.9
wave6	8.9	−3.7	12.6	2.2
wave7	10.3	−5.3	15.6	2.4
wave8	8.0	−3.2	11.2	3.5

than the troughs and asymmetric: the front face being significantly steeper than the back face. Most of them are followed by a secondary crest. Table 3 and figure 9 demonstrate that wave1 has the highest crest (12.9 m) with a shallow preceding trough (−6.1 m) and the largest individual wave height (19.0 m). The second highest wave (wave7) has a wave height reaches 15.6 m but with a lower wave trough (−5.3 m) and lower crest (10.3 m) than wave1. At the studied location (P_{SIS}), the time separating the preceding trough and the crest of wave1, which can be linked to the front face geometric steepness, is only 2.0 s, the lowest value among the different waves. The record of the back trough of wave1 is dominated by noise because of the water spray induced by the wave slamming that blinded the video cameras and corrupted the reconstruction for a short period of time. In figure 9, the grey bar indicates the elevation of the top of the lighthouse substructure, the bar thickness quantifies the water-level variation over the time period of the wave record, namely the water level dropped by 42 cm during the 30 min wave record considered. Measurements of a tide gauge from Shom collected at Le Conquet harbour (25 km ESE of La Jument) show storm surge values around 0 cm at 10.00 UTC the same day. We assumed here that the storm surge at La Jument can be neglected in our analysis. Figure 9 indicates that the crest elevation of wave1 measured at P_{SIS} is the only one crossing the substructure elevation level. We advance that this is a plausible explanation for the acceleration peak found for wave1 only. Since La Jument's tower is much more flexible than the substructure itself [4] the mechanical response to wave slamming impacts on the tower may be significantly more intense and may translate into much larger accelerations and displacements than those due to waves impacting the substructure only. This would explain why waves with slightly lower crest elevations, such as wave7, produced horizontal accelerations and displacements of the top of the structure one order of magnitude lower than wave1. Of course, it is difficult to be fully conclusive regarding the actual elevation of the crest right at the lighthouse, from considerations derived from observations collected at 50 m away from the structure. As reported earlier in the paper, the elevation can change significantly along the crest over distances of O(50 m) (figures 7 and 8, central panels). Because of the white water the near wave field (closer to 50 m in the up-wave direction) was not accessible from the SIS data. To fill the gap between the lighthouse and the edge of the SIS surface we operated BOSZ, a phase-resolving Boussinesq-type model for the computation of near-shore waves (e.g. [42–45]) that solves the equations based on a conserved variable formulation of [46]. Animations of the wave transformation in the vicinity of the lighthouse are available as electronic supplementary material. The computation of the wave field around the lighthouse of La Jument is based on a 2.7 km by 2.5 km domain composed of a Cartesian grid of uniform 7.5 m by 7.5 m. The input wave spectrum comes from the wave buoy at the time of interest, i.e. 3 January 2017 at 9.30.

As shown in figure 10, the wave field shows strong convergence in close proximity to the lighthouse with H_s values 50% higher than the observed offshore conditions. This suggests that, statistically speaking, wave height may be higher at the base of the lighthouse than at P_{SIS}, though

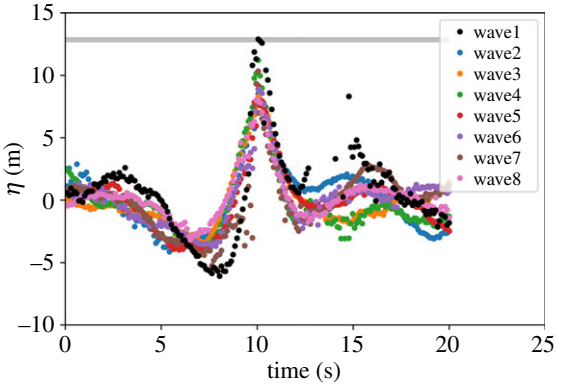

Figure 9. Comparison between wave1 (black) and the seven other high waves for the record of 3 January 2018 at 9.39 UTC. The grey bar indicated the altitude of the lighthouse substructure (figure 1) above the sea level at the time of the wave record. The vertical extent of the bar corresponds to the water level change over the 30 min of the record.

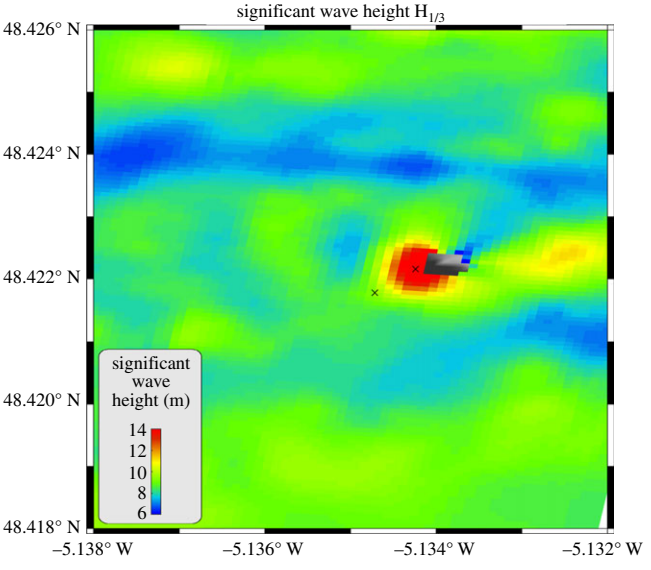

Figure 10. Significant wave height map obtained from the BOSZ model for the simulation corresponding to the wave event of 09.39 on 3 January.

the reflection of the wave field on the substructure likely contributes to this local wave height increase. However, even with this additional information, it is not possible to draw definitive conclusions regarding the elevation of wave1's crest on the structure since there is no guarantee that the observed statistical increase in H_s systematically results in higher individual wave crests.

Fortunately, a series of pictures of wave1 taken from Ushant Island supports our findings. These improbable but highly valuable pictures are available in [47] and present the details of wave1's impact on La Jument (for the review stage, a picture is available as electronic supplementary material). These pictures confirm that wave1 crest elevation was high enough to cause an impact above the substructure, i.e. directly on the tower. Two pieces of evidence match to relate the pictures to wave1: the correspondence of the time stamps is less than 2 min (probably due to inaccuracies in the camera clock) and wave1 was the only wave in our records of 3 January 2019 that caused sea spray up to the stereo-system. This finding confirms the numerical results

of Loraux, who reported that breaker impacts on the substructure alone do not produce any significant accelerations on La Jument (see fig. 46 in [4]). The substructure built several years after the lighthouse's erection plays therefore a double role: it adds stiffness to the initial lighthouse tower and protects it from the assaults of most of the breaking waves.

5. Discussion

The paper introduces a broad spectra of observational and model data that we used to provide a better understanding of the complex hydrodynamics in the vicinity of La Jument. However, the coming discussion will focus on the wave-acceleration study performed in the previous section.

The first analysis presented here examined a particular stereo-video record featuring a large breaking wave (wave1) that induced significant horizontal accelerations and displacements in the tower and caused water spray that reached up to the video cameras. As mentioned in the Introduction, the mechanical response of La Jument under extreme waves was addressed in detail by Loraux [4], who simulated the loading of a series of three waves with characteristics based on the estimation of 50–100 year return period waves, combined with varying tidal level. The horizontal acceleration and displacement caused by wave1 (looking at the x-axis) is of the same order or magnitude as the values report by Loraux's [4] numerical experiment, though his largest numerical wave (22 m high with crest elevation of 18 m) combined with a 8.5 m CD tidal level (50 cm above the highest astronomic tide and 6.5 m below the substructure top) yields a horizontal acceleration peak above $20\,\mathrm{m\,s^{-2}}$. Loraux further found that the horizontal displacements (up to 2 cm) were highly correlated to the duration of the impact pressure load.

We should stress here that the waves studied in our paper correspond to a severe but not extreme storm: indeed the significant wave height of 10.5 m is a wave event with a 2 year return period. In addition, the tide level was low (1.15 m CD in average over the 30 min record) which places the water level 12.85 m below the top of the lighthouse substructure. Even in these 'adverse' conditions, our instruments captured a wave able to hit the lighthouse's upper tower causing notable vibrations (double integration in time yields horizontal displacements of about 45 mm at the top of La Jument). This advocates for more observations in stronger sea states with different water levels to accumulate more acceleration data synchronized to wave observations. This would further help understanding the relation between the wave characteristics in terms of wave height, period and direction, the water level and the tidal currents on the impact magnitude on the structure. A larger subset of high waves reaching the tower would be necessary to examine what other properties (e.g. breaking type, breaking stage, angle of attack, fluid velocities in the crest) are important, beyond the crest elevation. In addition, since the stereo-video domain does not cover the last 50 m of wave propagation, additional sensors would be helpful in capturing the elevation of the wave impact on the structure. Numerical efforts to represent the three-dimensional geometry and fluid velocities of the impacting crest would also help in the cross interpretation of the wave characteristics especially regarding the distribution of the orbital velocities and their role in the impact process.

The acceleration records have only been briefly addressed in the paper and served just as markers of the wave slamming severity. These observations deserve a dedicated study, especially regarding their spectral contents that would provide important information about the stiffness of La Jument, hence its structural health and remaining lifetime.

We hope to further investigate the scientific questions raised in this discussion thanks to the extension of the field experiment over several winters and the addition of five pressure sensors, one on the substructure and four on the lighthouse tower, spread over three faces of the octagonal structure. We hope they will provide further information regarding the relation between impacting wave properties and the magnitude and time history of the pressure loads.

6. Conclusion

In this paper, we present observations from a field campaign designed to improve the description of the extreme wave loads on one of the most iconic lighthouse in France, if not in the world. The dataset, collected during winter 2017–2018, contains storm waves and wave-synchronized acceleration data together with tidal current measurements and high-resolution bathymetry. The dataset features several records with significant wave heights about 10 m for two of them and giant waves reaching 24 m high.

In the paper, we focused our analysis around an intense and isolated horizontal acceleration and displacement burst and showed that it is due to a 19 m high breaking wave. Our work suggests that this particular wave (wave1) carried a crest high enough to pass above the substructure and reach the lighthouse tower. A series of photographs of wave1 taken from Ushant island support that the crest hits the concrete belt covering the lower part of the tower [47]. This indicates that the water level during storm events controls the frequency of strong acceleration peaks since the lighthouse substructure acts as a high-pass filter for the wave crests. We hope that this ongoing field work will help in quantifying the remaining lifetime of La Jument through a finer description of the incoming waves and of their effect in terms of mechanical loading on the structure. This experiment could further bring insight regarding the loads of breaking waves on other marine structures installed on top of a steep slope such as breakwaters.

La Jument is a heritage iconic structure, part of Brittany's culture and known all over the world. Putting aside its role in the navigation safety, it is wise to wonder whether we should spend large amounts of money to maintain a monument that is not accessible to the public. Our scientific experiment demonstrates that this lighthouse is a unique laboratory to study extreme waves and the loading they induced on marine structures. We believe that its privileged location at the edge of a steep shoal overseeing the open ocean makes it a favourable site for many other fields of research including wave–current interactions, wave breaking or air–sea interface processes. This opportunity could offer a second operational life to La Jument and may justify maintaining this fascinating monument in good condition.

Data accessibility. This article does not contain any additional data.

Authors' contributions. J.F.F. drafted the manuscript and analysed the accelerations and stereo-video times series. P.G., F.L., M.A. and R.D. produced and analysed the stereo-video surfaces; E.L., N.F. and A.V. contributed to the accelerations analyses; M.P. did the hydrodynamic climatology study; J.H. and R.C. were in charge of the X-band investigations; C.R. was in charge the datawell and AWAC observation study; A.B. performed the rogue wave analysis; V.R. was responsible for the BOSZ modelling; M.F. and N.L.D. carried out the MBS field survey and analysed the bathymetric data.

Competing interests. We declare we have no competing interests.

Funding. This work benefited from government support managed by the Agence Nationale de la Recherche under the program Investissement d'Avenir with the reference ANR-10-IEED-0006-14 and ANR-10-IEED-0006-26 related to the projects DiMe and CARAVELE. Numerical simulations were performed on HPC facilities Datarmor of 'Pôle de Calcul Intensif pour la Mer' (PCIM) (http://www.ifremer.fr/pcim). Finally, the fundings from la filiére Mer, Crédit Agricole contributed to the success of the experiment.

Acknowledgements. We acknowledge the contribution of Peter Sutherland and (Ifremer) to the deployment of the stereo-system and assistance in the SIS data acquisition. We thank Lucia Pineau-Guillou (Ifremer) for her assistance in the storm surge data analysis. We are grateful to Phares et Balises who allows us to work on La Jument and provides significant support in the preparation and realization of the deployment. We would like to thank the reviewers whose comments have significantly improve the manuscript.

References

1. Fichou J-C, Le Hénaff N, Mével X. 1999 *Phares: histoire du balisage et de l'éclairage des côtes de France*. Douarnenez, France: Le chasse marees - ArMen.
2. Brownjohn J, Raby A, Bassitt J, Hudson E, Antonini A. 2017 Modal testing of offshore rock lighthouses around the british isles. *Procedia Eng.* **199**, 3326–3331. (doi:10.1016/j.proeng.2017.09.440)

3. Brownjohn JMW, Raby A, Bassitt J, Antonini A, Hudson E, Dobson P. 2018 Experimental modal analysis of british rock lighthouses. *Mar. Struct.* **62**, 1–22. (doi:10.1016/j.marstruc.2018.07.001)
4. Loraux C. 2013 Comportement structural des phares en mer, etude historique sur le phare de la jument et propositions d'intervention. Master's thesis, Maintenance Construction Sécurité (MCS), Ecole Polytechnique Fédérale de Lausanne. mcs.epfl.ch.
5. Morison JR, Johnson JW, Schaaf SA. 1950 The force exerted by surface waves on piles. *J. Pet. Technol.* **2**, 149–154. (doi:10.2118/950149-G)
6. Wienke J, Sparboom U, Oumeraci H. 2001 Breaking wave impact on a slender cylinder. In *Coastal engineering 2000* (ed. IJ Losada), pp. 1787–1798. Amsterdam, The Netherlands: Elsevier.
7. Perlin M, Choi W, Tian Z. 2013 Breaking waves in deep and intermediate waters. *Annu. Rev. Fluid Mech.* **45**, 115–145. (doi:10.1146/annurev-fluid-011212-140721)
8. Blenkinsopp CE, Chaplin JR. 2011 Void fraction measurements and scale effects in breaking waves in freshwater and seawater. *Coastal Eng.* **58**, 417–428. (doi:10.1016/j.coastaleng.2010.12.006)
9. Bredmose H, Bullock GN, Hogg AJ. 2015 Violent breaking wave impacts. Part 3. Effects of scale and aeration. *J. Fluid Mech.* **765**, 82–113. (doi:10.1017/jfm.2014.692)
10. Ma ZH, Causon DM, Qian L, Mingham CG, Mai T, Greaves D, Raby A. 2016 Pure and aerated water entry of a flat plate. *Phys. Fluids* **28**, 016104. (doi:10.1063/1.4940043)
11. Miche A. 1944 Mouvements ondulatoires de la mer en profondeur croissante ou décroissante. forme limite de la houle lors de son déferlement. application aux digues maritimes. Troisième partie. Forme et propriétés des houles limites lors du déferlement. Croissance des vitesses vers la rive. *Ann. Ponts et Chaussées Tome* **114**, 369–406.
12. Battjes JA, Janssen JPFM. 1978 Energy loss and set-up due to breaking of random waves. In *Proc. of the 16th Int. Conf. on Coastal Eng*, pp. 569–587. New York, NY: ASCE.
13. Barthelemy X, Banner ML, Peirson WL, Fedele F, Allis M, Dias F. 2018 On a unified breaking onset threshold for gravity waves in deep and intermediate depth water. *J. Fluid Mech.* **841**, 463–488. (doi:10.1017/jfm.2018.93)
14. Varing A, Filipot JF, Roeber V, Duarte R, Yates-Michelin M. 2018 A discussion on the wave breaking criterion of shallow water ocean waves. *Actes des 16eme Journees de l'Hydrodyanimque, 27–29 Novembre 2018, Centrale Marseille - IRPHE*. See http://website.ec-nantes.fr/actesjh/images/16JH/Articles/JH2018_papier_09C_Varing_et_al.pdf.
15. Thornton EB, Guza RT. 1983 Transformation of wave height distribution. *J. Geophys. Res.* **88**, 5925–5938. (doi:10.1029/JC088iC10p05925)
16. Iribarren CR, Nogales C. 1949 Protection des ports. In *xviith Int. Navigation Congress, Lisbon, Portugal*.
17. Hallowell S, Myers AT, Arwade SR. 2016 Variability of breaking wave characteristics and impact loads on offshore wind turbines supported by monopiles. *Wind Energy* **19**, 301–312. (doi:10.1002/we.1833)
18. Chella MA, Tørum A, Myrhaug D. 2012 An overview of wave impact forces on offshore wind turbine substructures. *Energy Procedia* **20**, 217–226. (doi:10.1016/j.egypro.2012.03.022)
19. Von Karman T. 1929 The impact on seaplane floats during landing. Technical note 321. US National Advisory Committee for Aeronautics.
20. Goda Y, Kakizaki S. 1966 Study on finite amplitude standing waves and their pressure upon a vertical wall. *Rept. Port Harbour Res. Inst.* **5**, 57.
21. Wienke J, Oumeraci H. 2005 Breaking wave impact force on a vertical and inclined slender pile—theoretical and large-scale model investigations. *Coastal Eng.* **52**, 435–462. (doi:10.1016/j.coastaleng.2004.12.008)
22. International Electrotechnical Commission IEC. 2009 IEC 61400-3. wind turbines–part 3: design requirements for offshore wind turbines. Technical Report.
23. DNV. 2014 Recommended Practice DNV-RP-C205: environmental conditions and environmental loads. Det Norske Veritas.
24. SHOM. 2017 Références altimétriques maritimes. côtes du zéro hydrographique et niveaux caractéristiques de la marée, service hydrographique et océanographique de la marine, brest. See https://diffusion.shom.fr/pro/risques/references-verticales/references-altimetriques-maritimes-ram.html.

25. Boudière E, Maisondieu C, Ardhuin F, Accensi M, Pineau-Guillou L, Lepesqueur J. 2013 A suitable metocean hindcast database for the design of marine energy converters. *Int. J. Mar. Energy* **3**, e40–e52. (doi:10.1016/j.ijome.2013.11.010)
26. Fedele, Francesco, Prasanna Sampath, Gallego G, Yezzi A, Benetazzo A, Forristall GZ, Tayfun MA, Cavaleri L, Sclavo M, Bastianini M. 2009 Beyond waves and spectra: Euler characteristics of oceanic sea states. In *Proc. the ASME 28th Inter. Conf. Off. Mech. Arc. Eng.*
27. Benetazzo A. 2006 Measurements of short water waves using stereo matched images sequences. *Coast. Eng.* **53**, 1013–1032. (doi:10.1016/j.coastaleng.2006.06.012)
28. Leckler F. 2013 Observation et modélisation du déferlement des vagues. PhD thesis, Brest.
29. Bergamasco F, Torsello A, Sclavo M, Barbariol F, Benetazzo A. 2017 Wass: an open-source pipeline for 3D stereo reconstruction of ocean waves. *Comput. Geosci.* **107**, 28–36. (doi:10.1016/j.cageo.2017.07.001)
30. Rodriguez JJ, Aggarwal JK. 1990 Stochastic analysis of stereo quantization error. *IEEE Trans. Pattern Anal. Mach. Intell.* **12**, 467–470. (doi:10.1109/34.55106)
31. Borge JCN, Reichert K, Dittmer J. 1999 Use of nautical radar as a wave monitoring instrument. *Coastal Eng.* **37**, 331–342. (doi:10.1016/S0378-3839(99)00032-0)
32. Carrasco R, Horstmann J, Seemann J. 2017 Significant wave height measured by coherent X-band radar. *IEEE Trans. Geosci. Remote Sens.* **55**, 5355–5365. (doi:10.1109/TGRS.2017.2706067)
33. Senet CM, Seemann J, Zeimer F. 2001 The near-surface current velocity determined from image sequences of the sea surface. *IEEE Trans. Geosci. Remote Sens.* **39**, 492–505. (doi:10.1109/36.911108)
34. Huang W, Carrasco R, Chengxi S, Gill EW, Horstmann J. 2016 Surface current measurements using X-band marine radar with vertical polarization. *IEEE Trans. Geosci. Remote Sens.* **54**, 2988–2996. (doi:10.1109/TGRS.2015.2509781)
35. Streßer M, Carrasco R, Horstmann J. 2017 Video-based estimation of surface currents using a low-cost quadcopter. *IEEE Geosci. Remote Sens. Lett.* **14**, 2027–2031. (doi:10.1109/LGRS.2017.2749120)
36. Lund B, Haus BK, Horstmann J, Graber HC, Carrasco R, Laxague NJM, Novelli G, Guigand CM, Özgökmen TM. 2018 Near-surface current mapping by shipboard marine X-band radar: a validation. *J. Atmos. Oceanic Technol.* **35**, 1077–1090. (doi:10.1175/JTECH-D-17-0154.1)
37. Benetazzo A, Serafino F, Bergamasco F, Ludeno G, Ardhuin F, Sutherland P, Sclavo M, Barbariol F. 2018 Stereo imaging and X-band radar wave data fusion: an assessment. *Ocean Eng.* **152**, 346–352. (doi:10.1016/j.oceaneng.2018.01.077)
38. Draper L. 1964 'freak' ocean waves. *Oceanus* **10**, 13–15.
39. Boccotti P. 1981 On the highest waves in a stationary Gaussian process. *Atti. Acc. Lig.* **38**, 45–73.
40. Phillips O, Gu D, Donelan M. 1993 Expected structure of extreme waves in a Gaussian sea. Part I: theory and SWADE buoy measurements. *J. Phys. Oceanogr.* **23**, 992–1000. (doi:10.1175/1520-0485(1993)023<0992:ESOEWI>2.0.CO;2)
41. Phillips O, Gu D, Walsh EJ. 1993 Expected structure of extreme waves in a Gaussian sea. Part II: SWADE scanning radar altimeter measurements. *J. Phys. Oceanogr.* **23**, 2297–2309. (doi:10.1175/1520-0485(1993)023<2297:OTESOE>2.0.CO;2)
42. Roeber V, Cheung KF, Kobayashi MH. 2010 Shock-capturing boussinesq-type model for nearshore wave processes. *Coastal Eng.* **57**, 407–423. (doi:10.1016/j.coastaleng.2009.11.007)
43. Roeber V, Cheung KF. 2012 Boussinesq-type model for energetic breaking waves in fringing reef environments. *Coastal Eng.* **70**, 1–20. (doi:10.1016/j.coastaleng.2012.06.001)
44. Roeber V, Bricker JD. 2015 Destructive tsunami-like wave generated by surf beat over a coral reef during typhoon haiyan. *Nat. Commun.* **6**, 7854. (doi:10.1038/ncomms8854)
45. Li N, Yamazaki Y, Roeber V, Cheung KF, Chock G. 2018 Probabilistic mapping of storm-induced coastal inundation for climate change adaptation. *Coastal Eng.* **133**, 126–141. (doi:10.1016/j.coastaleng.2017.12.013)
46. Nwogu O. 1993 Alternative form of boussinesq equations for nearshore wave propagation. *J. Waterway Port Coast. Ocean Eng.* **119**, 618–638. (doi:10.1061/(ASCE)0733-950X(1993)119:6(618))
47. Denarié E, Fady N. 2019 Structural response of French offshore heritage lighthouses. *Phil. Trans. R. Soc. A* **377**, 20190011. (doi:10.1098/rsta.2019.0011)